

Seismic performance of exoskeleton structures

*Original*

Seismic performance of exoskeleton structures / Reggio, Anna; Restuccia, Luciana; Martelli, Lucrezia; Ferro, Giuseppe Andrea. - In: ENGINEERING STRUCTURES. - ISSN 0141-0296. - 198:(2019), p. 109459.  
[10.1016/j.engstruct.2019.109459]

*Availability:*

This version is available at: 11583/2746672 since: 2019-08-07T16:17:19Z

*Publisher:*

elsevier

*Published*

DOI:10.1016/j.engstruct.2019.109459

*Terms of use:*

This article is made available under terms and conditions as specified in the corresponding bibliographic description in the repository

*Publisher copyright*

(Article begins on next page)

# Seismic performance of exoskeleton structures

Anna Reggio<sup>a,\*</sup>, Luciana Restuccia<sup>a</sup>, Lucrezia Martelli<sup>a</sup>, Giuseppe Andrea Ferro<sup>a</sup>

<sup>a</sup>*Department of Structural, Geotechnical and Building Engineering, Politecnico di Torino, Corso Duca degli Abruzzi 24, 10129 Torino, Italy*

---

## Abstract

Biomimetic exoskeleton structures are external self-supporting structural systems suitably connected to primary inner structures, the latter being enhanced or protected, in a general sense, by virtue of this connection. Their potential asset for an integrated retrofitting approach, combining structural safety and sustainability merit, has recently drawn considerable attention. In this work, the focus is on investigating the performance of exoskeleton structures as structural control systems under seismic loading. The exoskeleton structure is modelled as a dynamic system whose mass (in principle, not negligible), stiffness and damping properties can be varied and, possibly, designed with the aim of controlling the response of the primary structure. A non-dissipative, and in particular rigid, coupling is assumed between the primary structure and the exoskeleton structure. A first insight into the dynamic behaviour of the coupled system is gained in frequency domain. The dynamic equilibrium is set in non-dimensional form and the response to harmonic base motion is analysed with varying system parameters. Complex-valued Frequency Response Functions are used as performance evaluators in terms of relative displacement, absolute acceleration and transmitted force. A case study is subsequently discussed, dealing with the seismic response of a mid-rise reinforced concrete frame, designed with non-ductile behaviour, coupled to a steel diagrid-like lattice exoskeleton structure. Results of the seismic analyses show that the rigid coupling to the exoskeleton

---

\*Corresponding author.

*Email address:* [anna.reggio@polito.it](mailto:anna.reggio@polito.it) (Anna Reggio)

structure allows to achieve a significant displacement and deformation control of the primary structure, as well as important reductions of its internal forces, in terms of both base and floor shear forces.

*Keywords:* structural dynamics, structural control, exoskeleton structures, coupling, base motion, frequency response, seismic response

---

## 1. Introduction

Endowed with biomimetic meaning, the locution *exoskeleton structure* is used to indicate a self-supporting structural system set outside and suitably connected to a primary inner structure, the latter being enhanced or protected, in a general sense, by virtue of this connection. Attention has been recently drawn to the potential asset of exoskeleton structures for an integrated retrofitting approach, in which the structural safety as well as energy efficiency, environmental sustainability and architectural quality of existing buildings are improved in a combined and coordinated way [1, 2, 3].

In earthquake-prone regions, where innovative structural control technologies are crucial to the achievement of a resilient built environment [4, 5, 6, 7], the feasibility of exoskeleton structures for seismic protection is particularly worthy of being investigated [8]. In the present study, the exoskeleton structure is hence regarded as a structural control system that can be designed for the external seismic retrofitting of a building frame structure. External structural control systems, like reinforced concrete cores and walls [9, 10, 11], stepping and pinned rocking walls [12, 13, 14] and reaction towers [15, 16, 17], are considered in literature as a promising strategy due to a number of reasons: any service or business downtime, as well as residents displacement, is kept to a minimum because the retrofitting process is operated from outside of the building; interference with existing structural and nonstructural components is limited; the possible strengthening of structural members is restricted to the ones locally interested by the connections to the external control system. A number of specific advantages are further envisaged for exoskeleton structures: they can

25 boost both the economic and ecological efficiency of the retrofitting interven-  
tion, thanks to the above-mentioned potential for a multifunctional integrated  
design; depending on urban planning restrictions, they may either adhere to or  
be an expansion of the existing building, thereby allowing for additional housing  
spaces and increasing the real estate value; they foster the building technological  
30 updating and the urban regeneration [18, 19].

The aim of the present study is to explore the seismic performance of ex-  
oskeleton structures and their ability to reduce the earthquake-induced vibra-  
tions of existing structures. The consideration of an *intra*-connection between  
two subsystems of a same, single structural system is a distinctive aspect of this  
35 study and, compared to previous literature about the *inter*-connection between  
adjacent structures, it involves essential differences that have to be highlighted.

Most literature works on adjacent structures focus on new buildings, de-  
signed with given dynamic properties and subsequently coupled at storey level  
to limit structural damage or avoid pounding under dynamic loading. The  
40 coupling is electively dissipative, implementing viscous [20, 21], visco-elastic  
[22, 23, 24, 25] or hysteretic [26, 27, 28, 29] dampers, aimed at providing sup-  
plemental energy dissipation. A relative motion between the two structures is  
therefore essential and ensured by substantially different dynamic properties.  
The main issue discussed by these work is the design of the dissipative coupling  
45 [30, 31], generally optimised according to a global protection strategy, so that  
the overall response of both the coupled structures is reduced [11].

In this paper, the exoskeleton structure is conceived as a “sacrificial ap-  
pendage”, called to absorb seismic loads in order to increase the performance of  
a primary frame structure. A non-dissipative, and in particular rigid, coupling  
50 is assumed between the primary structure and the exoskeleton structure. The  
focus is on investigating how such a rigid coupling affects the dynamic response  
of the primary frame structure and whether it could be useful for vibration con-  
trol objectives under seismic loading. The approach of study is the most general  
one: given that, in principle, the mass of the exoskeleton structure is not negli-  
55 gible, dynamic coupling is fully taken into account; the exoskeleton structure is

modelled as a dynamic system whose properties, in terms of mass, stiffness and damping, can be varied and, possibly, designed with the aim of controlling the response of the primary structure.

The paper is arranged as follows. After the Introduction, the dynamic model  
60 of the system composed of two coupled linear viscoelastic oscillators is defined  
in Section 2: such a model is of interest, first, due to its paradigmatic value,  
and second, because it has been proved to be representative of the reduced-order  
modal model of coupled multi-degree-of-freedom structures [23]. The dynamic  
equilibrium of the coupled system is set in non-dimensional form, highlighting  
65 the governing independent parameters, and a parametric study is carried out in  
frequency domain on the response to harmonic base motion. The results, dis-  
cussed in Section 3, lead to characterise the dynamic behaviour of the coupled  
system and to discern the principle of operation delineated by the exoskeleton  
structure in terms of vibration control. A case study is subsequently presented  
70 in Section 4, dealing with the seismic response of a mid-rise reinforced con-  
crete frame structure, designed with non-ductile behaviour, coupled to a steel  
diagrid-like lattice exoskeleton structure. This choice was motivated by the con-  
sideration that diagrid systems are a structural typology particularly appealing  
for exoskeleton structures, thanks to their inherent structural efficiency, mor-  
75 phological versatility and architectural quality [32], as well as for the possible  
standardisation and replicability of components [33]. Conclusions are finally  
drawn in Section 5.

## 2. Structural model

Without lack of generality, the system composed of a primary structure con-  
nected to an exoskeleton structure is modelled by means of two coupled linear  
viscoelastic oscillators (Figure 1). The primary oscillator, with  $M_1$ ,  $K_1$  and  $C_1$   
as mass, stiffness and damping coefficients, represents the primary structure; the  
secondary oscillator, with  $M_2$ ,  $K_2$  and  $C_2$  as mass, stiffness and damping coeffi-  
cients, represents the exoskeleton structure; coupling between the two oscillators

is assumed to be non-dissipative and is modelled as a Hooke spring with stiffness coefficient  $K$ . When the system is excited by a base motion  $X_g(t)$ , the dynamic equilibrium is written with reference to relative displacements  $U_1 = X_1 - X_g$  and  $U_2 = X_2 - X_g$  as

$$M_1 U_1'' + C_1 U_1' + K_1 U_1 = -M_1 X_g'' + K(U_2 - U_1) \quad (1a)$$

$$M_2 U_2'' + C_2 U_2' + K_2 U_2 = -M_2 X_g'' - K(U_2 - U_1), \quad (1b)$$

with  $(\cdot)'$  denoting differentiation with respect to time  $t$ .

The limit case of the Hooke spring with the stiffness coefficient tending to infinity,  $K \rightarrow \infty$ , can be viewed as the case of a rigid coupling between primary and secondary oscillator. It follows  $U_2 \rightarrow U_1$  and, to the limit, Equations 1 are replaced by the equation of motion of a single-degree-of-freedom (sdof) system:

$$(M_1 + M_2)U_1'' + (C_1 + C_2)U_1' + (K_1 + K_2)U_1 = -(M_1 + M_2)X_g''. \quad (2)$$

To give a more general description of the problem, Equation 2 is rendered non-dimensional by scaling with respect to the chosen characteristic values of frequency  $\Omega_1 = \sqrt{K_1/M_1}$ , displacement  $U^* = M_1 g/K_1$  and force  $F^* = M_1 g$ , being  $\Omega_1$  the uncoupled natural frequency of the primary oscillator and  $g$  the acceleration due to gravity. Dimensionless variables  $\tau = \Omega_1 t$  and  $u_1 = U_1/U^*$  are thus defined and Equation 2 is set in non-dimensional form as

$$(1 + \mu)\ddot{u}_1 + (2\zeta_1 + 2\zeta_2\alpha\mu)\dot{u}_1 + (1 + \alpha^2\mu)u_1 = -(1 + \mu)\ddot{x}_g, \quad (3)$$

with the overdot indicating differentiation with respect to dimensionless time  $\tau$ .

Relevant independent parameters in (3) are:

$$\mu = \frac{m_2}{m_1}, \quad \alpha = \frac{\Omega_2}{\Omega_1}, \quad \zeta_1 = \frac{c_1}{2\sqrt{k_1 m_1}}, \quad \zeta_2 = \frac{c_2}{2\sqrt{k_2 m_2}}. \quad (4)$$

80 The mass ratio and the frequency ratio between the two oscillators are denoted by  $\mu$  and  $\alpha$ , respectively, with  $\Omega_2$  being the uncoupled natural frequency of the secondary oscillator;  $\zeta_1$  and  $\zeta_2$  are the uncoupled damping ratios of the primary and of the secondary oscillator; non-dimensional base acceleration  $\ddot{x}_g$  results to be scaled by gravity.

85 **3. Frequency response**

We characterise the dynamic behaviour of the coupled primary-secondary oscillator system in frequency domain, a representation that is natural and effective when dealing with the performance of structural control strategies [34, 35, 36]. Complex-valued Frequency Response Functions (FRFs) are defined and  
 90 used as performance evaluators for each response quantity of interest: coupled system displacement  $u_1$  relative to the base and absolute acceleration  $\ddot{x}_1$ ; force  $f$  transmitted from the moving base to the mass of the coupled system.

*3.1. Displacement and acceleration response*

Base motion and the steady-state relative displacement of the coupled system are assumed to be harmonic with same non-dimensional circular frequency  $\omega = \Omega/\Omega_1$ . They are represented as rotating vectors in Gauss-Argand plane as:

$$x_g(\tau) = x_{g0}e^{i\omega\tau}, \quad u_1(\tau) = u_{10}e^{i\omega\tau}, \quad (5)$$

with  $x_{g0}$  and  $u_{10}$  being complex amplitudes with different phases. By introducing the assumed harmonic functions (5) into the equation of motion (3), a FRF can be defined as the ratio between the amplitude of the system relative displacement,  $u_{10}$ , and the amplitude of base acceleration,  $\ddot{x}_{g0}$ :

$$H_{u_1\ddot{x}_g}(\omega) = \frac{u_{10}}{\ddot{x}_{g0}} = -\frac{(1 + \mu)}{1 + \alpha^2\mu + i\omega(2\zeta_1 + 2\zeta_2\alpha\mu) - \omega^2(1 + \mu)}. \quad (6)$$

If a harmonic function is introduced, instead, for the system absolute displacement,  $x_1(\tau) = x_{10}e^{i\omega\tau}$ , a FRF can be defined as the ratio between the amplitude of the system absolute acceleration,  $\ddot{x}_{10}$ , and the amplitude of base acceleration,  $\ddot{x}_{g0}$ :

$$H_{\ddot{x}_1\ddot{x}_g}(\omega) = \frac{\ddot{x}_{10}}{\ddot{x}_{g0}} = \frac{(1 + \alpha^2\mu) + i\omega(2\zeta_1 + 2\zeta_2\alpha\mu)}{1 + \alpha^2\mu + i\omega(2\zeta_1 + 2\zeta_2\alpha\mu) - \omega^2(1 + \mu)}. \quad (7)$$

In Figure 2, the magnitude of the FRFs for both the relative displacement  
 95 and the absolute acceleration of the coupled system are plotted versus the excitation frequency  $\omega$ ; to comparison purposes, the magnitude of the corresponding

FRFs of the uncoupled primary oscillator is shown as well. Within the set of parameters (4) governing the dynamic behaviour of the coupled system,  $\mu = 0.05$ ,  $\zeta_1 = 0.05$  and  $\zeta_2 = 0.05$  are fixed, while frequency ratio  $\alpha$  is varied in the range [0.1, 10]: increments of frequency ratio  $\alpha$ , for a constant mass ratio  $\mu$ , correspond to the stiffening of the secondary oscillator with respect to the primary oscillator. As a first result, the peak of FRFs, which denotes the natural frequency of the coupled system, is progressively shifted towards higher frequency values. A second observation is that, as  $\alpha$  increases, the peak magnitude considerably decreases for the relative displacement FRF, while it slightly increases for the absolute acceleration FRF.

In consideration of the above results, parametric analyses are carried out to thoroughly explore the influence of rigid coupling on the dynamic response of the primary oscillator. Two response ratios are defined in terms of FRF peak magnitude:

$$R_{u_1} = \frac{\max |H_{u_1 \ddot{x}_g}(\omega)|^C}{\max |H_{u_1 \ddot{x}_g}(\omega)|^U}, \quad R_{\ddot{x}_1} = \frac{\max |H_{\ddot{x}_1 \ddot{x}_g}(\omega)|^C}{\max |H_{\ddot{x}_1 \ddot{x}_g}(\omega)|^U}, \quad (8)$$

where superscripts C and U denote, respectively, the Coupled primary-secondary oscillator system and the Uncoupled primary oscillator. Based on definitions (8), values of  $R_{u_1}$  or  $R_{\ddot{x}_1}$  smaller than one imply a reduction of the resonance response of the primary oscillator, in terms of relative displacement or absolute acceleration, by virtue of the rigid coupling to the secondary oscillator. Parameters to be studied are the mass ratio  $\mu$  and the frequency ratio  $\alpha$ , which can be considered as the design parameters of the coupled system. Damping ratios  $\zeta_1$  and  $\zeta_2$ , conversely, are taken as given properties of the oscillators, both equal to 0.05. Results are presented in Figure 3 for  $\mu$  ranging from 0.01 to 0.20 and  $\alpha$  ranging from 0.1 to 10.

Although minima are non found, it appears from Figures 3(a) that  $R_{u_1}$  assumes values lower than one in a large part of the spanned parameters space, indicating that the displacement response of the primary oscillator can be significantly reduced by way of the rigid coupling to the secondary oscillator; in particular,  $R_{u_1} < 1$  when  $\alpha > 1$ . Figures 3(b) show, however, that, where the

displacement response is reduced, the acceleration response is amplified instead ( $R_{\ddot{x}_1} > 1$ ), a drawback that should be carefully taken into account when dealing with vibration control objectives. It is worth noting that, for  $\mu > 0.10$ ,  $R_{u_1}$  appears to be more sensitive to variations in frequency ratio  $\alpha$  than in mass ratio  $\mu$ : it means that, even with a limited mass, but proper dynamic properties, the coupled secondary oscillator is able to effectively control the displacement response of the primary oscillator.

### 3.2. Transmitted force

A response quantity of interest in the base excitation problem is the force transmitted to the mass of the system due to the motion of the base [37]. From the free-body diagram in Figure 1(b), the force transmitted to the mass of the coupled system is the sum of the forces through the springs and dampers,  $F = (K_1 + K_2)U_1 + (C_1 + C_2)U_1'$ . By resorting to non-dimensional form and assuming the system harmonic response  $u_1(\tau)$  given in (5), it becomes:

$$f(\tau) = (1 + \alpha^2\mu)u_{10}e^{i\omega\tau} + i\omega(2\zeta_1 + 2\zeta_2\alpha\mu)u_{10}e^{i\omega\tau} = f_0e^{i\omega\tau}. \quad (9)$$

A FRF can be defined as the ratio between the amplitude of the transmitted force,  $f_0$ , and the amplitude of base acceleration,  $\ddot{x}_{g0}$ :

$$H_{f\ddot{x}_g}(\omega) = \frac{f_0}{\ddot{x}_{g0}} = (1 + \alpha^2\mu + i\omega 2\zeta_1 + i\omega 2\zeta_2\alpha\mu) H_{u_1\ddot{x}_g}(\omega), \quad (10)$$

being  $H_{u_1\ddot{x}_g}(\omega)$  the relative displacement FRF introduced in Equation (6).

Since the two coupled oscillators are set in parallel, it is possible to split the total transmitted force (9) into the sum of the forces transmitted through each oscillator:

$$f(\tau) = f_1(\tau) + f_2(\tau) = f_{10}e^{i\omega\tau} + f_{20}e^{i\omega\tau}. \quad (11)$$

Consequently,

$$H_{f_1\ddot{x}_g}(\omega) = \frac{f_{01}}{\ddot{x}_{g0}} = (1 + i\omega 2\zeta_1) H_{u_1\ddot{x}_g}(\omega) \quad (12)$$

and

$$H_{f_2\ddot{x}_g}(\omega) = \frac{f_{02}}{\ddot{x}_{g0}} = (\alpha^2\mu + i\omega 2\zeta_2\alpha\mu) H_{u_1\ddot{x}_g}(\omega) \quad (13)$$

are the FRFs measuring the amplitude of the forces transmitted, per unit base acceleration, through the primary and the secondary oscillator, respectively.

Comparisons concerning the transmitted forces are drawn in Figure 4 . As in Figure 2, for the coupled system, parameters  $\mu = 0.05$ ,  $\zeta_1 = 0.05$  and  $\zeta_2 = 0.05$  are given, while frequency ratio  $\alpha$  ranges from 0.1 to 10. Figure 4(a) shows that the peak magnitude of the total transmitted force FRF,  $H_{f\ddot{x}_g}(\omega)$ , is greater in the coupled system than in the uncoupled primary oscillator and is increased by increasing  $\alpha$ . However, by considering individually the contribution through each oscillator,  $H_{f_1\ddot{x}_g}(\omega)$  and  $H_{f_2\ddot{x}_g}(\omega)$ , a twofold effect becomes apparent: increments of  $\alpha$  lead to a reduction in the peak transmitted force through the primary oscillator (Figure 4(b)) and, meanwhile, to an increase in the peak transmitted force through the secondary oscillator (Figure 4(c)). To quantify such variations in the transmitted force proportions, two ratios are defined in terms of FRF peak magnitude:

$$R_{f_1} = \frac{\max |H_{f_1\ddot{x}_g}(\omega)|^C}{\max |H_{f_1\ddot{x}_g}(\omega)|^U}, \quad R_{f_2} = \frac{\max |H_{f_2\ddot{x}_g}(\omega)|^C}{\max |H_{f_1\ddot{x}_g}(\omega)|^U}, \quad (14)$$

where, as before, superscripts C and U denote the Coupled system and the Uncoupled primary oscillator, respectively. In Figures 5,  $R_{f_1}$  and  $R_{f_2}$  are plotted  
135 by varying parameters mass ratio  $\mu$  and frequency ratio  $\alpha$ . Results indicate that, by selecting  $\alpha > 1$ , the rigid coupling to the secondary oscillator is able to reduce the peak transmitted force through the primary oscillator ( $R_{f_1} < 1$ ) (Figures 5(a)). Such reductions increase by increasing  $\alpha$  and  $\mu$  and imply the simultaneous rise of the peak force through secondary oscillator (Figures 5(b)).

#### 140 4. Case study

The parametric analyses discussed in Section 3 indicate that the resonance response of a primary oscillator, subjected to base motion, can be reduced, as to both relative displacement and internal forces, by way of the rigid coupling to a secondary oscillator, if the dynamic properties of the latter are purposely  
145 selected. In this section, we deal with the seismic response of multi-degree-of-

freedom frame structures and a case study is presented to explore how it could be affected by the rigid coupling to an exoskeleton structure.

#### 4.1. Primary structure

A benchmark primary structure, located in a high seismicity site and not  
150 complying with the seismic performance requirements of current Italian Building  
Code [38], is considered. It consists of a 4-storey, 4 bays by 2 bays, reinforced  
concrete moment-resisting frame designed with non-ductile behaviour. Constant  
span length and inter-storey height are  $l = 6$  m and  $h = 3.50$  m, respectively,  
with global dimensions of 24 m x 12 m x 14 m in the longitudinal ( $x$ ), transverse  
155 ( $y$ ) and vertical ( $z$ ) directions. Distributions of mass and stiffness are uniform  
in plan and in elevation: columns and beams cross-sections are rectangular with  
dimensions 40x40 cm and 40x30 cm, respectively; total floor mass is equal to  
240.24 kNs<sup>2</sup>/m. The structure is therefore symmetrical in plan with respect to  
both the  $x$ - and  $y$ -direction. A Finite Element (FE) model (Figure 6 (a)) has  
160 been developed by employing the OpenSees [39] module within the structural  
analysis program CDS WIN [40] . Floor slabs have been verified to have an  
in-plane rigid behaviour, entailing the introduction of a diaphragm constraint  
at each floor level.

#### 4.2. Exoskeleton structure

165 A self-supporting exoskeleton structure, adjacent to the primary structure,  
is subsequently considered for retrofitting purposes (Figure 6 (b)). It consists  
of a diagrid-like structural system made of S235 steel columns and diagonal  
beams, whose cross-sections are HE100A and 114.3 mm x 5 mm circular hollow,  
respectively; the beam inclination angle is 49°. In the FE model of the coupled  
170 system, the exoskeleton structure is connected to the primary structure at each  
floor level by means of rigid links, preserving overall regularity in plan and in  
elevation.

### 4.3. Modal properties

Modal properties of the bare primary structure (i.e., in the absence of the  
175 exoskeleton structure) and of the coupled primary-exoskeleton system are re-  
ported in Table 1. In both cases, plans have two orthogonal axes of symmetry,  
the longitudinal  $x$ -axis and the transverse  $y$ -axis. Purely bending and perfectly  
decoupled vibration modes are therefore obtained, while torsional modes are  
evidenced by null participating mass ratios.

180 Broadly speaking, natural frequencies of the coupled system are higher than  
the ones of the bare primary structure. This effect is more pronounced as to the  
first two modes and in the longitudinal direction rather than in the transverse  
direction: the first natural frequency (i.e., first bending mode in transverse  
 $y$ -direction) increases by 86%, from 7.051 to 13.093 rad/s (the corresponding  
185 period dropping from 0.891 to 0.480 s); the second natural frequency (i.e., first  
bending mode in longitudinal  $x$ -direction) increases by 129%, from 7.521 to  
17.190 rad/s (the corresponding period dropping from 0.835 to 0.366 s). It is  
worth observing that also the participating mass ratios vary between the bare  
primary structure and the coupled system. Specifically, they increase in the first  
190 two vibration modes and decrease in all the other modes: for the first mode,  
 $M_y$  grows from 83.92% to 88.49%; for the second mode,  $M_x$  grows from 84.50%  
to 90.76%; for all the other modes, reductions of either  $M_y$  or  $M_x$  are obtained.

### 4.4. Seismic analyses

Response spectrum analyses are carried out on the FE models of the bare  
195 primary structure and of the coupled primary-exoskeleton system, with the aim  
of comparing their performance under earthquake loading. Seismic input is de-  
scribed by pseudo-acceleration response spectra according to the Italian Build-  
ing Code [38]. A high seismicity site with soil class C (deposit of medium-dense  
sand) is considered and two seismic hazard levels are selected, defined in terms  
200 of reference peak ground acceleration at bedrock  $a_g$ : 1.  $a_g = 0.082g$ , with  
probability of exceedance of 63% in 50 years (mean return period 50 years),  
corresponding to the Damage Limitation (DL) performance requirement; 2.

$a_g = 0.249g$ , with probability of exceedance of 10% in 50 years (mean return period 475 years), corresponding to the Life Safety (LS) performance requirement. The relevant elastic pseudo-acceleration response spectra (5% viscous damping) are shown in Figure 7. Seismic action components are applied independently along each horizontal direction,  $x$  and  $y$ , evaluating separately the effects on the structural response [38, 41].

#### 4.5. Seismic response

Response quantities monitored in the seismic analyses are floor displacements relative to ground, inter-storey drifts and floor shear forces: from the viewpoint of seismic protection, they represent the engineering demand parameters which structural integrity and serviceability depend on.

Tables 2 and 3 report the peak floor displacements ( $U_x, U_y$ ) and inter-storey drifts ( $\Delta_x, \Delta_y$ ) obtained for the bare primary structure and for the coupled primary-exoskeleton system under the two levels of seismic excitation (DL and LF limit states). The variation of floor displacements over the height of the primary structure, both without and with the rigid coupling to the exoskeleton structure, is illustrated in Figure 8 for the LF limit state; in a similar way, Figure 9 depicts the profiles of inter-storey drift ratios, referring to an inter-storey height of 3.50 m, for the DL state. In both Figures 8 and 9, the graphs on the left plot the peak response values, while a performance index (PI) is presented on the right, in order to assess comparatively the control performance at various elevations. Such indices are defined as the ratio of the peak floor responses between the coupled primary-exoskeleton system and the bare primary structure: a value of PI smaller than one implies a reduction of the floor response in the coupled system as compared to the primary structure; conversely, a value greater than one means an amplification.

Due to the predominant contribution of the first vibration mode in both  $x$ - and  $y$ - direction, peak values of floor relative displacements (Figure 8 (a)) grow along the height of the primary structure and this trend is found for the coupled primary-exoskeleton system as well. For the bare primary structure, peak floor

displacements in the two horizontal directions are comparable, while for the coupled system, they are clearly smaller in the longitudinal ( $x$ ) than in the transverse ( $y$ ) direction, indicating a differential control effectiveness exerted by the exoskeleton structure. Looking at PI (Figure 8 (b)), reductions of peak floor displacements range from 55% to 67% in  $x$ -direction and from 33% to 51% in  $y$ -direction, increasing with the increasing floor level. Slightly lower reductions are obtained for the DL state, as reported in Table 2.

Peak inter-storey drift ratios for the bare primary structure are below 4‰, under DL state (Table 2), while they rise up to 10.5‰ and 11.2‰, corresponding to the second floor, under LS limit state (Table 3). For the coupled system, considerable reductions are observed, and particularly over the mid-storeys (second and third floor), where peak drifts are reduced by about 75% in  $x$ -direction and about 55% in  $y$ -direction, under both levels of seismic excitation. Profiles in Figure 9 show that a significant deformation control, although maximum at mid-storeys, is achieved over the entire height of the primary structure.

In addition to displacement and deformation control, the rigid coupling to the exoskeleton structure leads also to important reductions of the internal forces in the primary structure. Tables 4 and 5 report the peak floor shear forces ( $V_x$ ,  $V_y$ ) obtained for the bare primary structure and for the coupled primary-exoskeleton system under DL and LF limit states. As shown in Figure 10, base shear on the primary structure is reduced in the coupled system as compared to its bare configuration, but differences are found between the horizontal directions and the two levels of seismic excitation: under DL state, reductions amount to 38% in  $x$ -direction and 8% in  $y$ -direction; under LS limit state, reductions amount to 43% in  $x$ -direction and 17% in  $y$ -direction. The more the base shear on the primary structure is reduced, the higher the base shear on the exoskeleton structure is: while in  $y$ -direction, the base shear on the exoskeleton structure is lower than the one on the primary structure, in  $x$ -direction, the former is greater than the latter and almost comparable to the base shear on the bare primary structure. A comprehensive assessment, though, cannot leave aside the distribution of internal forces along the height

of the coupled system. Profiles of peak floor shear forces on the primary and  
265 on the exoskeleton structure are hence illustrated in Figure 11, normalised by  
dividing by the corresponding peak base shear on the bare primary structure. It  
is observed that shear forces on the primary structure appear to be reduced at all  
floor levels, although the greater reductions are found on the second and third  
floors, resulting in a significantly different distribution compared to the bare  
270 configuration. On the exoskeleton structure, shear forces are generally higher  
than on the primary structure and even comparable to the values characterising  
the bare primary structure.

## 5. Conclusions

This exploratory study was aimed at investigating whether exoskeleton struc-  
275 tures can be a viable and effective means to control structural response under  
seismic loading. The exoskeleton structure is conceived as a dynamic system  
whose mass, stiffness and damping properties can be varied and, possibly, de-  
signed in order to modify the response of a primary structure, connected by way  
of a rigid coupling.

280 Frequency domain analyses have been used to characterise the dynamic be-  
haviour of a coupled primary-secondary oscillator system and to discern the  
principle of operation delineated by the exoskeleton structure in terms of vibra-  
tion control. The dynamic equilibrium of the coupled system has been set in  
non-dimensional form, to identify the governing independent parameters, and  
285 a parametric study has been carried out on the response to harmonic base mo-  
tion. Ratios in terms of FRF peak magnitude have shown that the resonance  
response of the primary oscillator can be reduced, as to both displacements and  
internal forces, by virtue of the rigid coupling to the secondary oscillator, if the  
dynamic properties of the latter are purposely selected.

290 Seismic analyses have been subsequently conducted on a case study in which  
a mid-rise reinforced concrete frame structure, designed with non-ductile be-  
haviour, is rigidly connected at each floor level to an exoskeleton structure,

realised as a steel diagrid-like lattice structure. By comparing the seismic response of the bare primary structure and of the coupled primary-exoskeleton system, the following results emerge:

- a significant displacement and deformation control of the primary structure is achieved: peak floor displacements are reduced, on average, by 40%–50%, while reductions of peak inter-storey drifts are higher and up to 75%;
- although floor displacements and inter-storey drifts are reduced over the entire height of the primary structure, the maximum control effectiveness is found at mid-storeys;
- in addition to displacement and deformation control, important reductions of the internal forces in the primary structure are also obtained, in terms of both base and floor shear forces; distribution of floor shear forces along the height of the primary structure appear to be significantly different compared to the bare configuration;
- the more the internal forces on the primary structure are reduced, the higher the internal forces on the exoskeleton are; broadly speaking, floor shear forces on the exoskeleton structure are found to be comparable to the values denoting the bare primary structure;
- a differential control effectiveness is found between the longitudinal and the transverse horizontal direction, due to the different dynamic properties exhibited by the connected primary and exoskeleton structure in the two directions.

Future research should address the optimal design problem of the exoskeleton structures, according to a multi-objective optimisation approach taking into account both the control performance and the cost of the retrofitting strategy. The introduction of supplemental damping, viscous or hysteretic, provided by the exoskeleton structure would be of interest and should be dealt with.

## Acknowledgements

This research work was partially funded by the Italian Civil Protection Department under project RELUIS-DPC 2014-2018. Anna Reggio and Luciana Restuccia are also grateful to Politecnico di Torino for the financial support received in the form of a Starting Grant for Young Researchers (grants 57\_ATEN\_RSG16REGANN and 57\_ATEN\_RSG18RESLUC).

## References

- [1] A. Caverzan, M. Lamperti Tornaghi, P. Negro (Eds.), Proceedings of SAFESUST Workshop. A roadmap for the improvement of earthquake resistance and eco-efficiency of existing buildings and cities, Publications Office of the European Union, 2016. doi:10.2788/499080.
- [2] A. Marini, C. Passoni, P. Riva, P. Negro, E. Romano, F. Taucer, Technology options for earthquake resistant, eco-efficient buildings in Europe: Research needs. EUR 26497 EN JRC87425, Technical Report, Publications Office of the European Union, 2014. doi:10.2788/68902.
- [3] A. Belleri, A. Marini, Does seismic risk affect the environmental impact of existing buildings?, *Energy and Buildings* 110 (2016) 149–158.
- [4] G. W. Housner, L. A. Bergman, T. K. Caughey, A. G. Chassiakos, R. O. Claus, S. F. Masri, R. E. Skelton, T. T. Soong, B. F. Spencer, J. T. P. Yao, Structural controls past present future, *Journal of Engineering Mechanics* 123 (1997) 897–971.
- [5] B. F. Spencer, S. Nagarajaiah, State of the Art of Structural Control, *Journal of Structural Engineering* 129 (2003) 845–856.
- [6] M. Nakashima, O. Lavan, M. Kurata, Y. Luo, Earthquake engineering research needs in light of lessons learned from the 2011 Tohoku earthquake, *Earthquake Engineering and Engineering Vibration* 13 (2014) 141–149.

- [7] T. E. Saaed, G. Nikolakopoulos, J.-E. Jonasson, H. Hedlund, A state-of-the-art review of structural control systems, *Journal of Vibration and Control* 21 (2015) 919–937.
- 350 [8] A. Reggio, L. Restuccia, G. A. Ferro, Feasibility and effectiveness of exoskeleton structures for seismic protection, *Procedia Structural Integrity* 9 (2018) 303–310.
- [9] T. Trombetti, S. Silvestri, Novel schemes for inserting seismic dampers in shear-type systems based upon the mass proportional component of the Rayleigh damping matrix, *Journal of Sound and Vibration* 302 (2007) 355 486–526.
- [10] O. Lavan, D. Abecassis, Seismic Behavior and Design of Wall–EDD–Frame Systems, *Frontiers in Built Environment* 1 (2015) 1–17.
- [11] R. Greco, G. C. Marano, Optimum design of viscous dissipative links in wallframe systems, *The Structural Design of Tall and Special Buildings* 25 360 (2016) 412–428.
- [12] Z. Qu, A. Wada, S. Motoyui, H. Sakata, S. Kishiki, Pin-supported walls for enhancing the seismic performance of building structures, *Earthquake Engineering & Structural Dynamics* 41 (2012) 2075–2091.
- 365 [13] N. Makris, M. Aghagholizadeh, The dynamics of an elastic structure coupled with a rocking wall, *Earthquake Engineering & Structural Dynamics* 46 (2017) 945–962.
- [14] M. Aghagholizadeh, N. Makris, Earthquake response analysis of yielding structures coupled with vertically restrained rocking walls, *Earthquake 370 Engineering & Structural Dynamics* (2018) 1–20.
- [15] A. Balducci, Dissipative Towers. Application n. EP2010074723820100831, WO2010EP62748 20100831, International and European classification E04H9/02; Italian concession n. 0001395591., 2005.

- [16] N. Impollonia, A. Palmeri, Seismic performance of buildings retrofitted  
375 with nonlinear viscous dampers and adjacent reaction towers, *Earthquake  
Engineering & Structural Dynamics* (2018) 1–23.
- [17] L. Gioiella, E. Tubaldi, F. Gara, L. Dezi, A. Dall’Asta, Modal proper-  
ties and seismic behaviour of buildings equipped with external dissipative  
pinned rocking braced frames, *Engineering Structures* 172 (2018) 807–819.
- 380 [18] L. Restuccia, T. Rosso, Smar-To: from the urban reconnection to the smart  
grid. Urban, energy and structural renovation of an existing building. Mas-  
ter’s Thesis, Politecnico di Torino, 2012.
- [19] A. Marini, C. Passoni, A. Belleri, F. Feroldi, M. Preti, G. Metelli, P. Riva,  
E. Giuriani, G. Plizzari, Combining seismic retrofit with energy refurbish-  
385 ment for the sustainable renovation of RC buildings: a proof of concept,  
*European Journal of Environmental and Civil Engineering* 8189 (2017) 1–  
21.
- [20] J. E. Luco, F. C. P. De Barros, Optimal damping between two adjacent  
elastic structures, *Earthquake Engineering & Structural Dynamics* *Struc-*  
390 *tural Dynamics* 27 (1998) 649–659.
- [21] E. Tubaldi, Dynamic behavior of adjacent buildings connected by linear  
viscous/viscoelastic dampers, *Structural Control and Health Monitoring*  
22 (2015) 1086–1102.
- [22] Y. L. Xu, Q. He, J. M. Ko, Dynamic response of damper-connected adjacent  
395 buildings under earthquake excitation, *Engineering Structures* 21 (1999)  
135–148.
- [23] T. Aida, T. Aso, K. Takeshita, T. Takiuchi, T. Fujii, Improvement of the  
structure damping performance by interconnection, *Journal of Sound and  
Vibration* 242 (2001) 333–353.
- 400 [24] J. Kim, J. Ryu, L. Chung, Seismic performance of structures connected by  
viscoelastic dampers, *Engineering Structures* 28 (2006) 183–195.

- [25] V. Gattulli, F. Potenza, M. Lepidi, Damping performance of two simple oscillators coupled by a visco-elastic connection, *Journal of Sound and Vibration* 332 (2013) 6934–6948.
- 405 [26] Y. Q. Ni, J. M. Ko, Z. G. Ying, Random seismic response analysis of adjacent buildings coupled with non-linear hysteretic dampers, *Journal of Sound and Vibration* 246 (2001) 403–417.
- [27] A. V. Bhaskararao, R. S. Jangid, Seismic analysis of structures connected with friction dampers, *Engineering Structures* 28 (2006) 690–703.
- 410 [28] M. Basili, M. De Angelis, Optimal passive control of adjacent structures interconnected with nonlinear hysteretic devices, *Journal of Sound and Vibration* 301 (2007) 106–125.
- [29] S. D. Bharti, S. M. Dumne, M. K. Shrimali, Seismic response analysis of adjacent buildings connected with MR dampers, *Engineering Structures* 32 (2010) 2122–2133.
- 415 [30] K. S. Park, S. Y. Ok, Optimal design of actively controlled adjacent structures for balancing the mutually conflicting objectives in design preference aspects, *Engineering Structures* 45 (2012) 213–222.
- [31] V. Gattulli, F. Potenza, B. F. Spencer, Design criteria for dissipative devices in coupled oscillators under seismic excitation, *Structural Control and Health Monitoring* (2018) e2167.
- 420 [32] V. Tomei, M. Imbimbo, E. Mele, Optimization of structural patterns for tall buildings: The case of diagrid, *Engineering Structures* 171 (2018) 280–297.
- 425 [33] S. Labò, C. Passoni, A. Marini, A. Belleri, G. Camata, P. Riva, E. Spacone, Prefabricated responsive diagrid for holistic renovation of existing mid-rise RC buildings, in: *Proceedings of COMPDYN 2017 - 6th ECCOMAS Thematic Conference on Computational Methods in Structural Dynamics*

- and Earthquake Engineering, Rhode Island, Greece, 2017, pp. June 15–17.  
430 doi:10.7712/120117.
- [34] B. F. Spencer, J. Suhardjo, M. Sain, Frequency domain optimal control strategies for aseismic protection, *Journal of Engineering Mechanics ASCE* 120 (1994) 135–158.
- [35] C. M. Harris, A. G. Piersol, T. L. Paez, *Harris’ Shock and Vibration Hand-*  
435 *book*, 6th ed., McGraw-Hill, New York, USA, 2010.
- [36] G. Genta, *Vibration Dynamics and Control*, Springer, 2009.
- [37] D. Inman, *Engineering Vibration*, 4th ed., Pearson Prentice Hall, Upper Saddle River, NJ, USA, 2014.
- [38] Ministero delle Infrastrutture e dei Trasporti, *Norme Tecniche per le*  
440 *Costruzioni*, D.M. 17.01.2018, Rome, 2018.
- [39] F. McKenna, G. Fenves, M. Scott, B. Jeremic, *Open system for earthquake engineering simulation (OpenSees)*, version 2.4.6, Pacific Earthquake Engineering Research Center, University of California at Berkeley, USA, 2013.
- [40] STS, *CDS Win Documentation*, [www.stsweb.it](http://www.stsweb.it), 2018.
- 445 [41] European Committee for Standardization (CEN), *Eurocode 8: Design of structures for earthquake resistance Part. 1: General rules, seismic actions and rules for buildings*, EN 1998-1., Brussels, 2004.

FIGURES

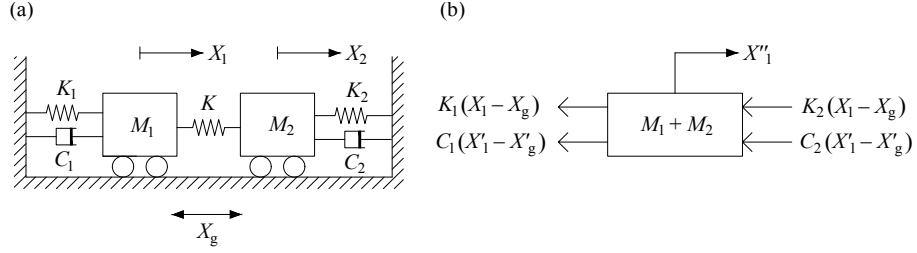


Figure 1: Coupled primary-secondary oscillator system: (a) structural model; (b) free body diagram in case of rigid coupling ( $K \rightarrow \infty$ ).

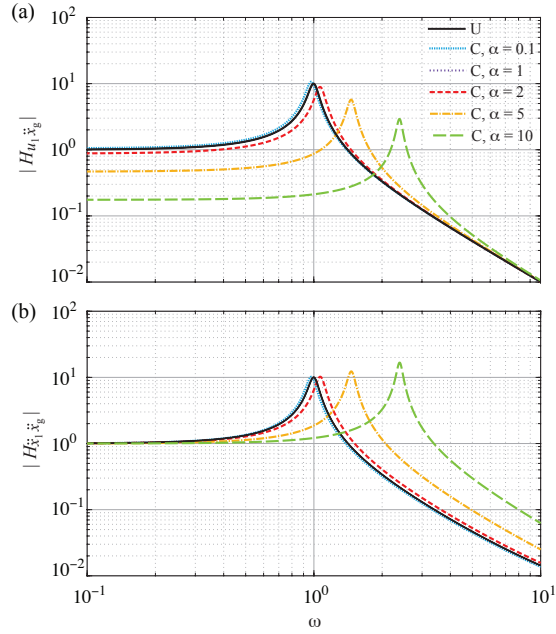


Figure 2: Magnitude of the FRFs (a)  $H_{u_1 \ddot{x}_g}$  of relative displacement and (b)  $H_{\ddot{x}_1 \ddot{x}_g}$  of absolute acceleration, for the Uncoupled (U) primary oscillator and for the Coupled (C) system with varying frequency ratio  $\alpha$ . It is assumed  $\mu = 0.05$ ,  $\zeta_1 = 0.05$  and  $\zeta_2 = 0.05$ .

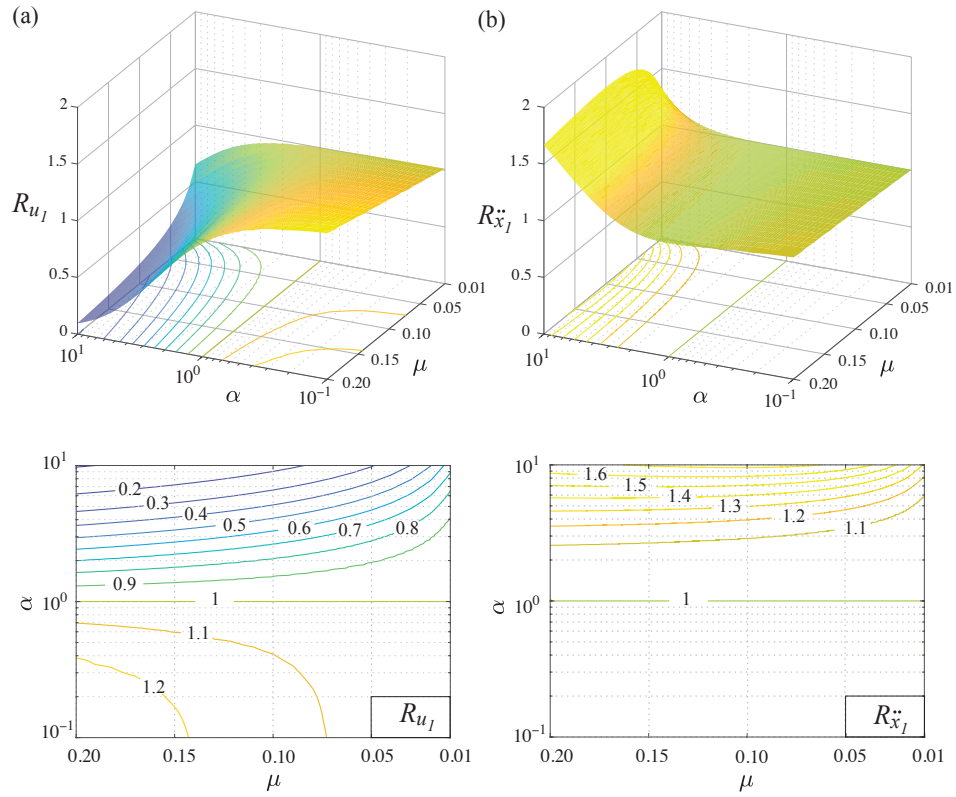


Figure 3: Surface and contour plots of response ratios, (a)  $R_{u_1}$  for relative displacement and (b)  $R_{\ddot{x}_1}$  for absolute acceleration, versus mass ratio  $\mu$  and frequency ratio  $\alpha$ . It is assumed  $\zeta_1 = 0.05$  and  $\zeta_2 = 0.05$ .

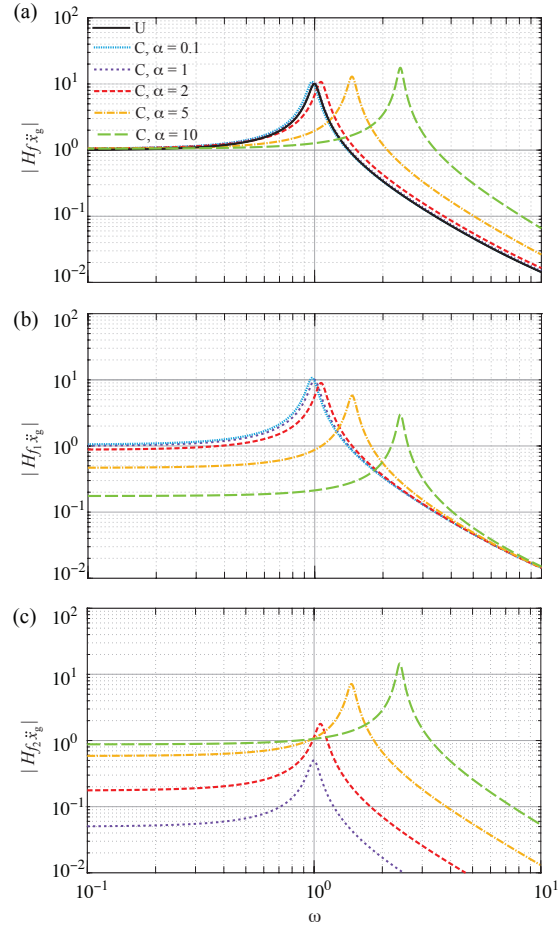


Figure 4: Magnitude of the FRFs (a)  $H_{f\ddot{x}_g}$  of total transmitted force, (b)  $H_{f_1\ddot{x}_g}$  of force transmitted through primary oscillator and (c)  $H_{f_2\ddot{x}_g}$  of force transmitted through secondary oscillator, for the Uncoupled (U) primary oscillator and for the Coupled (C) system with varying frequency ratio  $\alpha$ . It is assumed  $\mu = 0.05$ ,  $\zeta_1 = 0.05$  and  $\zeta_2 = 0.05$ .

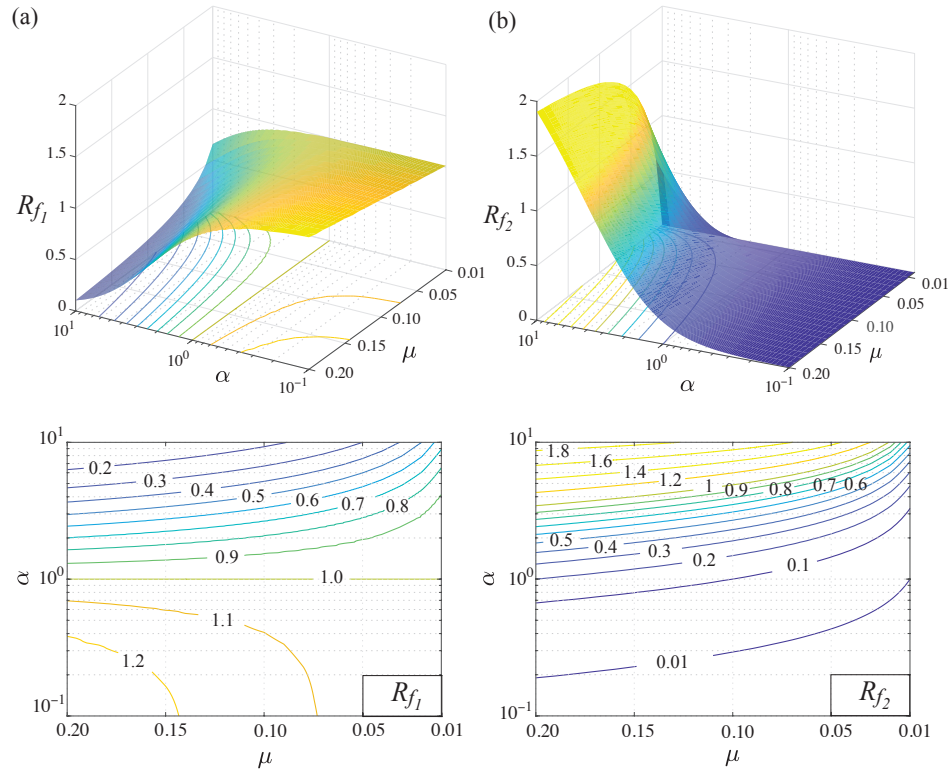


Figure 5: Surface and contour plots of transmitted force ratios, (a)  $R_{f_1}$  for the force through the primary oscillator and (b)  $R_{f_2}$  for the force through the secondary oscillator, versus mass ratio  $\mu$  and frequency ratio  $\alpha$ . It is assumed  $\zeta_1 = 0.05$  and  $\zeta_2 = 0.05$ .

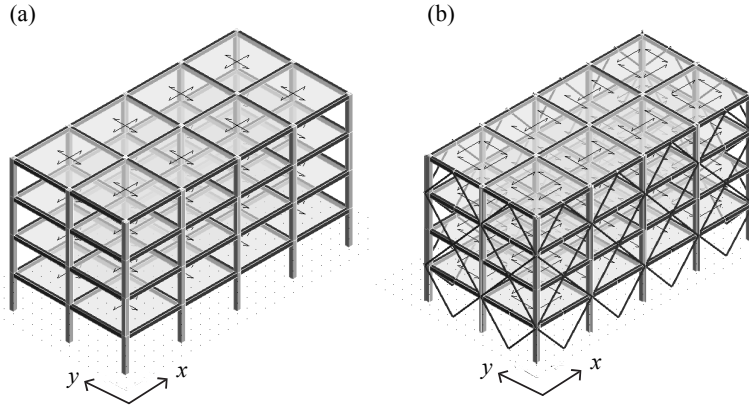


Figure 6: Three-dimensional views of the FE models of (a) the bare primary structure and (b) the coupled primary-exoskeleton system.

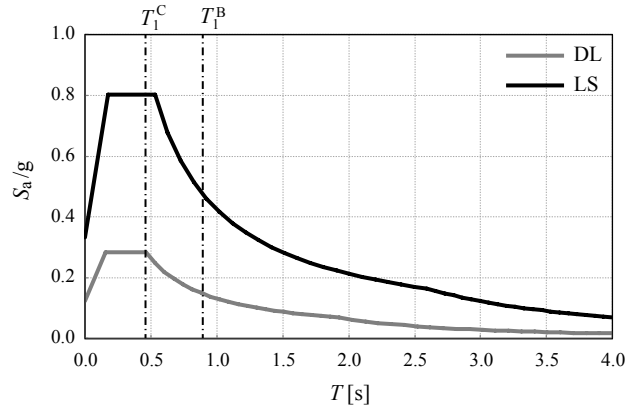


Figure 7: Elastic pseudo-acceleration response spectra (5% viscous damping) defined for the Damage Limitation (DL) and Life Safety (LS) performance requirements, according to the Italian Building Code [38]. Dash-dot lines indicate the fundamental vibration period of the Bare primary structure ( $T_1^B = 0.891$  s) and of the Coupled primary-exoskeleton system ( $T_1^C = 0.480$  s).

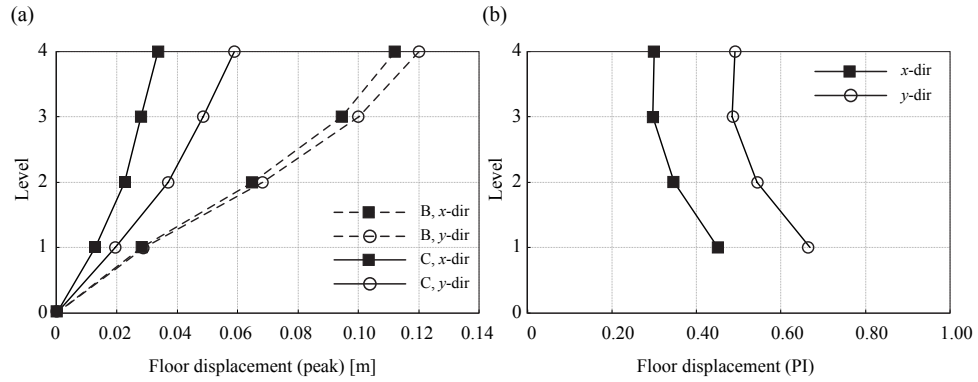


Figure 8: Profiles of floor displacements in  $x$ - and  $y$ -direction: (a) peak values for the Bare primary structure (B) and for the Coupled primary-exoskeleton system (C); (b) Performance Indices (PI). Life Safety limit state.

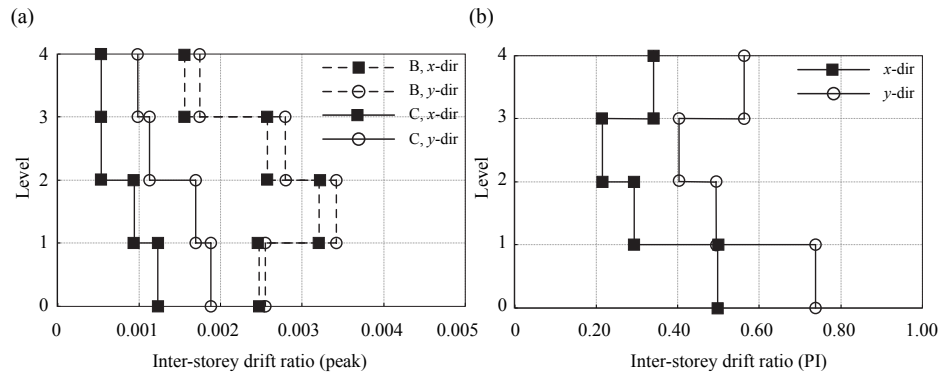


Figure 9: Profiles of inter-storey drift ratios in  $x$ - and  $y$ -direction: a) peak values for the Bare primary structure (B) and for the Coupled primary-exoskeleton system (C); (b) Performance Indices (PI). Damage Limitation state.

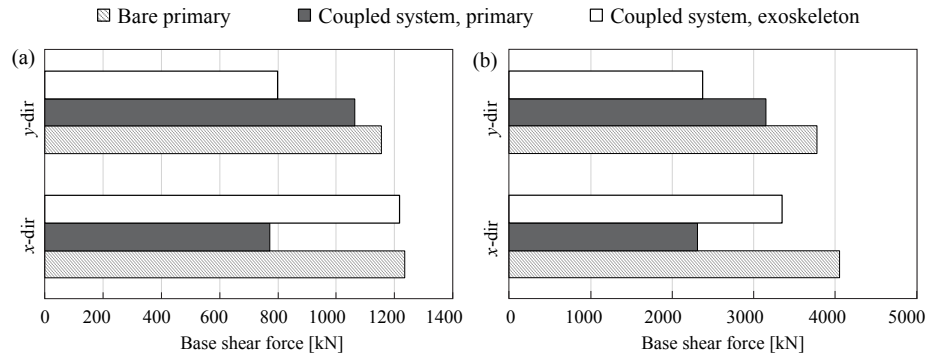


Figure 10: Peak base shear forces at (a) Damage Limitation state and (b) Life Safety limit state: comparison between bare primary structure and coupled primary-exoskeleton system.

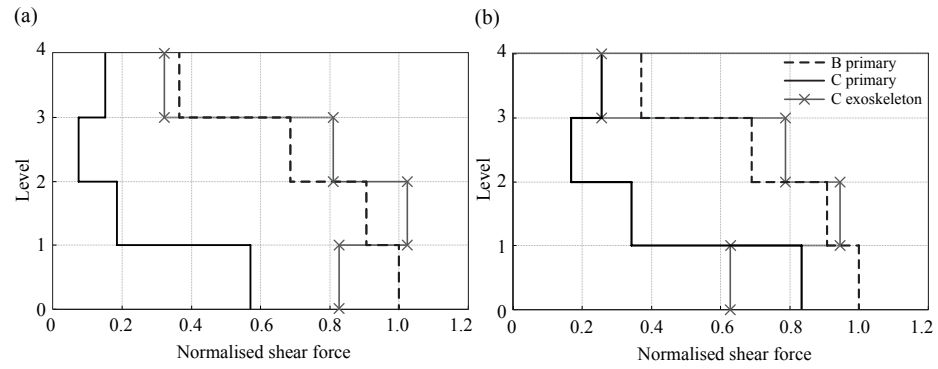


Figure 11: Profiles of normalised peak floor shear forces in (a)  $x$ - and (b)  $y$ -direction: comparison between Bare (B) primary structure and Coupled (C) primary-exoskeleton system. Life Safety limit state.

TABLES

Mode	Bare primary structure				Coupled primary-exoskeleton system			
	$\Omega$ [rad/s]	$T$ [s]	$M_x$ [%]	$M_y$ [%]	$\Omega$ [rad/s]	$T$ [s]	$M_x$ [%]	$M_y$ [%]
1	7.051	0.891	0.00	83.92	13.093	0.480	0.00	88.49
2	7.521	0.835	84.53	0.00	17.190	0.366	90.76	0.00
3	8.226	0.764	0.00	0.00	22.345	0.281	0.00	0.00
4	23.372	0.269	0.00	11.04	36.639	0.171	0.00	7.71
5	24.520	0.256	10.73	0.00	45.858	0.137	5.96	0.00
6	26.879	0.234	0.00	0.00	58.214	0.108	0.00	0.00
7	44.571	0.141	0.00	3.94	68.354	0.092	0.00	2.80
8	45.789	0.137	3.74	0.00	82.744	0.076	2.44	0.00
9	50.643	0.124	0.00	0.00	87.110	0.072	0.00	1.00
10	67.630	0.093	0.00	1.10	97.434	0.064	0.84	0.00
11	68.192	0.092	1.01	0.00	103.530	0.061	0.00	0.00
12	76.243	0.082	0.00	0.00	119.519	0.053	0.00	0.00

Table 1: Modal properties of the bare primary structure and of the coupled primary-exoskeleton system: circular frequencies  $\Omega$ , periods  $T$ , participating mass ratios in  $x$ -,  $M_x$ , and in  $y$ -direction,  $M_y$ .

Level	Bare primary structure				Coupled primary-exoskeleton system			
	$U_x$	$U_y$	$\Delta_x$	$\Delta_y$	$U_x$	$U_y$	$\Delta_x$	$\Delta_y$
	[m]	[m]	[%o]	[%o]	[m]	[m]	[%o]	[%o]
1	0.009	0.009	2.5	2.5	0.004	0.007	1.2	1.9
2	0.020	0.021	3.2	3.4	0.008	0.013	0.9	1.7
3	0.029	0.031	2.6	2.8	0.009	0.016	0.5	1.1
4	0.034	0.009	1.6	1.7	0.011	0.020	0.5	1.0

Table 2: Peak floor displacements ( $U_x$ ,  $U_y$ ) and inter-storey drift ratios ( $\Delta_x$ ,  $\Delta_y$ ) in  $x$ - and  $y$ -direction for the bare primary structure and for the coupled primary-exoskeleton system, Damage Limitation state.

Level	Bare primary structure				Coupled primary-exoskeleton system			
	$U_x$	$U_y$	$\Delta_x$	$\Delta_y$	$U_x$	$U_y$	$\Delta_x$	$\Delta_y$
	[m]	[m]	[%o]	[%o]	[m]	[m]	[%o]	[%o]
1	0.028	0.029	8.1	8.3	0.013	0.019	3.6	5.6
2	0.065	0.068	10.5	11.2	0.023	0.037	2.8	5.0
3	0.094	0.100	8.4	9.1	0.028	0.049	1.6	3.3
4	0.112	0.120	5.1	5.7	0.034	0.059	1.6	3.0

Table 3: Peak floor displacements ( $U_x$ ,  $U_y$ ) and inter-storey drift ratios ( $\Delta_x$ ,  $\Delta_y$ ) in  $x$ - and  $y$ -direction for the bare primary structure and for the coupled primary-exoskeleton system, Life Safety limit state.

Level	Bare primary structure		Coupled primary-exoskeleton system			
	$V_x$ [kN]	$V_y$ [kN]	$V_{x, \text{prim}}$ [kN]	$V_{x, \text{exo}}$ [kN]	$V_{y, \text{prim}}$ [kN]	$V_{y, \text{exo}}$ [kN]
1	1236	1154	771	1218	1063	799
2	1118	1048	253	1470	434	1204
3	846	797	104	1155	207	1010
4	453	426	212	460	326	327

Table 4: Peak floor shear forces ( $V_x, V_y$ ) in  $x$ - and  $y$ -direction for the bare primary structure and for the coupled primary-exoskeleton system, Damage Limitation state.

Level	Bare primary structure		Coupled primary-exoskeleton system			
	$V_x$ [kN]	$V_y$ [kN]	$V_{x, \text{prim}}$ [kN]	$V_{x, \text{exo}}$ [kN]	$V_{y, \text{prim}}$ [kN]	$V_{y, \text{exo}}$ [kN]
1	4053	3773	2311	3347	3146	2371
2	3669	3426	749	4152	1287	3567
3	2779	2605	299	3283	634	2972
4	1481	1394	612	1299	966	968

Table 5: Peak floor shear forces ( $V_x, V_y$ ) in  $x$ - and  $y$ -direction for the bare primary structure and for the coupled primary-exoskeleton system, Life Safety limit state.